© 2018 IJSRST | Volume 4 | Issue 8 | Print ISSN: 2395-6011 | Online ISSN: 2395-602X
Themed Section: Science and Technology

Fuzzy Logic Controller based SRM Drive for EVs with Flexible Energy Control Functions

N Jayabharath Reddy [1], M. Purusotham [2]

[1]PG Student / Department of Electrical & Electronic Engineering, SHREE Institute of Technical Education, Thirupati, Andhra Pradesh, India

[2]Associate Professor / Department of Electrical & Electronics Engineering, SHREE Institute of Technical Education, Thirupati, Andhra Pradesh, India

ABSTRACT

In this paper Hybrid Electric vehicle (HEV) technology provides an effective solution for achieving higher fuel economy and better performances with reduced greenhouse gas emissions. For Electric vehicle applications, To increase the driving miles of the electric vehicles, a photovoltaic (PV) panel is mounted along with on-board battery bank. A tri-port converter with fuzzy logic controller is proposed in this paper to control the energy flow between the PV panel, battery and SRM drive. Six operational modes are presented, four of which are developed for driving modes and rest two for stand still on-board charging. In driving modes, the Perturb and observe technique is employed in order to receive maximum power from the PV panel. In stand still charging modes, a grid connected charging topology is developed. A multi section charging control strategy is used foe effective utilization of energy in case of battery charging from PV panel directly. The proposed tri-port technology with fuzzy logic controller is developed in MATLAB/SIMULINK environment and the results are proven to be successful in producing reduced harmonic distortion .

Keywords: Electric Vehicles, Photovoltaic (PV), Switched Reluctance Motors (SRMs), Tri-Port Converter, Perturb and Observe Technique, Fuzzy Logic Controller.

I. INTRODUCTION

Electric vehicles have taken a significant leap forward, by advances in motor drives, power converters, batteries and energy management systems [1]-[4]. Be that as it may, due to the limitation of current battery technologies, the driving miles is moderately short that limits the wide utilization of EVs [5]-[7]. In terms of motor drives, high-performance permanent-magnet (PM) machines are generally utilized while rare-earth materials are required in large quantities, restricting the wide utilization of EVs. Keeping in mind the end goal to defeat these issues, a photovoltaic panel and a switched reluctance motor (SRM) are introduced with give power supply and motor drive, respectively. Firstly, by including the PV panel on top of the EV, a sustainable energy source is achieved. Nowadays, a typical passenger car has a surface enough to install a 250-W PV panel. Second, a SRM needs no rare-earth PMs and is additionally robust so it gets increasing attention in EV applications. While PV panels have low power density for traction drives, they can be used to charge batteries the greater part of time. For the most part, the PV-fed EV has a comparable structure to the hybrid electrical vehicle, whose internal combustion engine(ICE) is supplanted by the PV panel. The PV-fed EV system is outlined in Figure 1. Its key components include an off-board charging station, a PV, batteries and power converters. In order to decrease the energy conversion processes, one approach is to upgrade the motor to include some on-board charging functions. For example, paper designs

a 20-kW split-phase PM motor for EV charging, yet it endures from high harmonic contents in the back electromotive drive (EMF). Another solution depends on a traditional SRM. Paper achieves on-board charging and power factor correction in a 2.3-kW SRM by utilizing machine windings as the input filter inductor. The concept of modular structure of driving topology is proposed in paper. Based on intelligent power modules (IPM), a four-phase half bridge converter is utilized to achieve driving and grid-charging. In spite of the fact that modularization supports mass production, the utilization of half/full bridge topology reduces the system reliability (e.g. shoot-through issues). Paper builds up a basic topology for plug-in hybrid electrical vehicle (HEV) that supports flexible energy flow. In any case, for grid charging, the grid should be associated with the generator rectifier that builds the energy conversion process and decreases the charging efficiency. In any case, a powerful topology and control strategy for PV-fed EVs is not yet developed. Since the PV has different characteristics to ICEs, the maximum power point tracking (MPPT) and solar energy utilization are the unique factors for the PV-fed EVs.

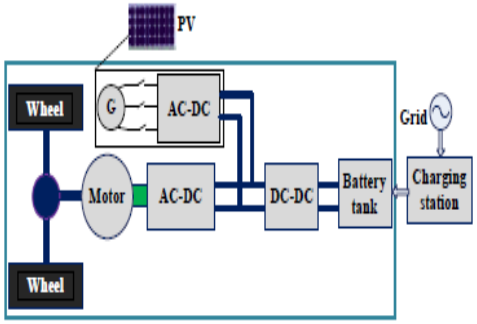

Figure 1. PV-fed hybrid electrical vehicle.

In order to achieve low cost and flexible energy flow modes, a low cost tri-port converter is proposed in this paper to arrange the PV panel, SRM and battery. Six operational modes are developed to support flexible control of energy flow.

II. TOPOLAGY AND OPERATIONAL MODES

A. Proposed topology and working modes

The proposed Tri-port topology has three energy terminals, PV, battery and SRM. They are linked by a power converter which comprises of four switching devices (S0~S3), four diodes (D0~D3) and two relays, as appeared in Figure 2 [26]. By controlling relays J1 and J2, the six operation modes are upheld, as appeared in Figure 3; the corresponding relay activities are delineated in Table I. In mode 1, PV is the energy source to drive the SRM and to charge the battery. In mode 2, the PV and battery are both the energy sources to drive the SRM. In mode 3, the PV is the source and the battery is idle. In mode 4, the battery is the driving source and the PV is idle. In mode 5, the battery is charged by a single-phase grid while both the PV and SRM are idle. In mode 6, the battery is charged by the PV and the SRM is idle.

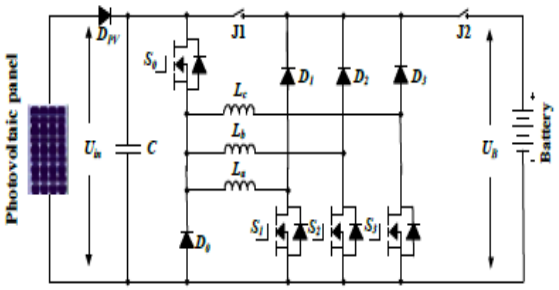

Figure 2. The proposed Tri-port topology for PV-powered SRM drive.

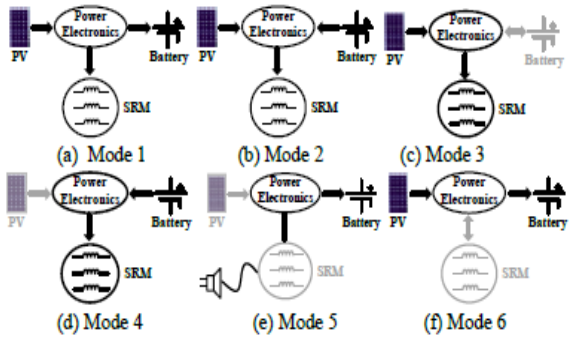

Figure 3. Six operation modes of the proposed Tri-port topology.

B. Driving modes

Working modes 1~4 are the driving modes to give traction drive to the vehicle.

(1) Mode 1

At light loads of operation, the energy produced from the PV is more than the SRM required; the system works in mode 1. The corresponding operation circuit is appeared in Fig.4 (an), The PV panel energy feed the energy to SRM and charge the battery; so in this mode, the battery is charged in EV operation condition.

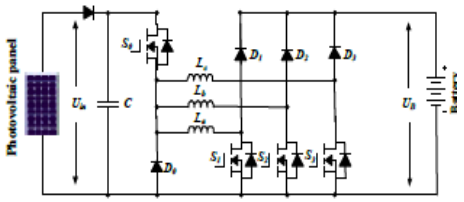

(a) Operation circuit under mode 1

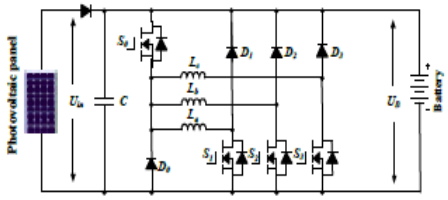

(b) Operation circuit under mode 2

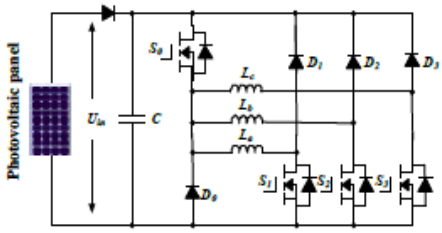

(c) Operation circuit under mode 3

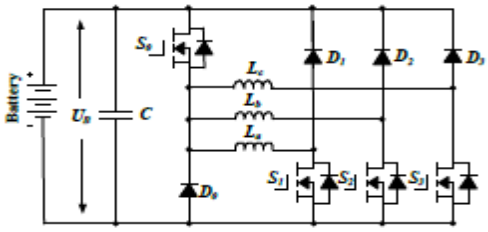

(d) Operation circuit under mode 4

Figure 4. the equivalent circuits under driving modes.

(2) Mode 2

At the point when the SRM operates in heavy load, for example, uphill driving or acceleration, both the PV panel and battery supply power to the SRM. The relating operation circuit is appeared in Figure 4(b).

(3) Mode 3

At the point when the battery is out of power, the PV panel is the only energy source to drive the vehicle. The corresponding circuit is appeared in Figure 4(c).

(4) Mode 4

At the point when the PV can't generate electricity due to low solar irradiation, the battery supplies power to the SRM. The corresponding topology is delineated in Figure 4(d). In this mode.

C. Battery charging modes

Operating modes 5 and 6 are the battery charging modes.

(5) Mode 5

At the point when PV can't generate electricity, an external power source is expected to charge the battery, for example, AC grid. The relating circuit is appeared in Figure 5(a). One of the three phase windings is split and its midpoint is pulled out, as appeared in Figure 5(a). Phase windings La1 and La2 are employed as input filter inductors. These inductors are a part of the drive circuit to form an AC-DC rectifier for grid charging.

(6) Mode 6

At the point when the EV is stopped under the sun, the PV can charge the battery The relating charging circuit is appeared in Figure 5(b).

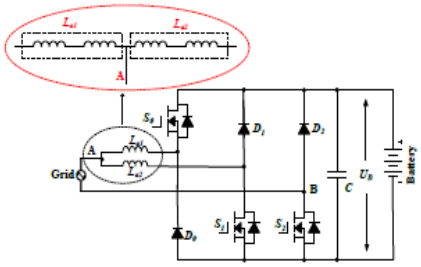

(a) Grid charging mode

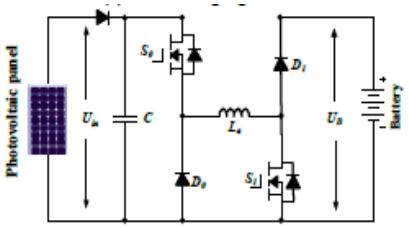

(b) PV source charging mode

Figure 5 Equivalent circuits of charging condition modes.

III. CONTROL STRATEGY UNDER DIFFERENT MODES

In order to make the best utilization of sun oriented energy for driving the EV, a control strategy under various modes is planned.

A. Single source driving mode

As indicated by the distinction in the power sources, there are PV-driving; battery-driving and PV and battery parallel fed source. In a heavy load condition, the PV power can't support the EV, mode 2 can be adopted to support enough energy and make full utilization of solar energy. Figure 6(a) demonstrates the equivalent power source; the corresponding PV panel working points is represented in Figure 6(b). Since the PV is paralleled with the battery, the PV panel voltage is clamped to the battery voltage UB. In mode 2, there are three working states: winding excitation, energy recycling and freewheeling states, as appeared in Figure 7. Modes 3 and 4 have comparable working states to mode 2. The difference is that the PV is the only source in mode 3 while the battery is the only source in mode 4.

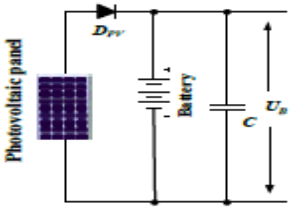

(a) Compound power source

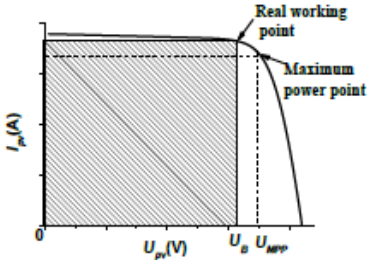

(b) Working point of the PV

Figure 6 Power supply at mode 2.

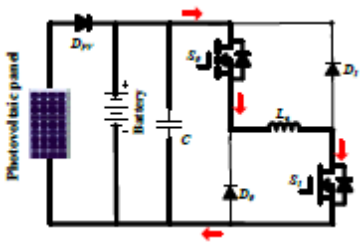

(a) Winding excitation state

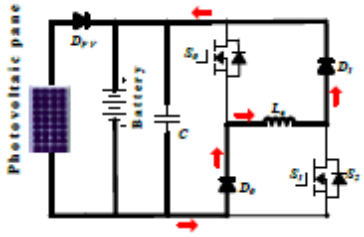

(b) Energy recycling state

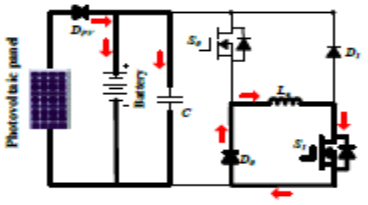

(c) Freewheeling state

Figure 7. Working states at mode 2.

Neglecting the voltage drop over the power switches and diodes, the phase voltage is given by

$$U_{in} = R_k i_k + \frac{d\psi(i_k,\theta_r)}{dt} = R_k i_k + L_k \frac{di_k}{dt} + i_k \omega_r \frac{dL_k}{d\theta_r}, \quad k = a,b,c \tag{1}$$

where Uin is the DC-link voltage, k is phase a, b, or c, Rk is the phase resistance, ik is the phase current, Lk is the phase inductance, θr is the rotor position, ψ(ik, θr) is the phase flux linkage depending upon the phase current and rotor position, and ωr is the angular speed. The third term in Eq. 1 is the back electromotive force (EMF) voltage by

$$e_k = i_k \omega_r \frac{dL_k}{d\theta_r} \tag{2}$$

Consequently, the phase voltage is found by

$$U_k = R_k i_k + L_k \frac{di_k}{dt} + e_k \tag{3}$$

In the excitation area, turning on S0 and S1 will induce a current in phase a winding, as show in Figure 7(a). Phase a winding is subjected to the positive DC bus voltage.

$$+U_{in} = R_k i_k + L_k \frac{di_k}{dt} + e_k \quad (4)$$

At the point when S0 is off and S1 is on, the phase current is in a freewheeling state in a zero voltage loop, as appeared in Figure 7(c), the phase voltage is zero.

$$0 = R_k i_k + L_k \frac{di_k}{dt} + e_k \quad (5)$$

In the demagnetization region, S0 and S1 are both turned off; what's more, the phase current will flow back to the power supply, as appear in Figure 7(b). In this state, the phase winding is subjected to the negative DC bus voltage, and the phase voltage is

$$-U_{in} = R_k i_k + L_k \frac{di_k}{dt} + e_k \quad (6)$$

In single source driving mode, the voltage-PWM control is utilized as the fundamental plan, as showed in Figure 8. As per the given speed ω*, the voltage-PWM control is activated at speed control.

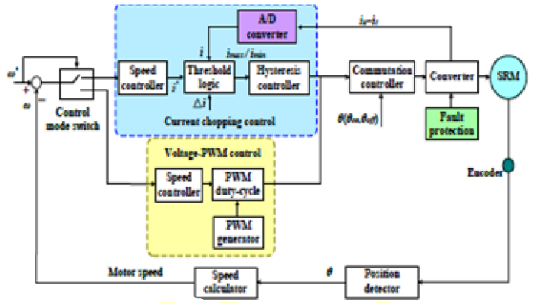

Figure 8. SRM control strategy under single source driving mode.

B. Driving-charging hybrid control strategy

In the driving-charging hybrid control, the PV is the driving source and the battery is charged by the freewheeling current, as represented in drive mode 1. There are two control targets: maximum power point tracking (MPPT) of the PV panel and speed control of the SRM. The dual-source condition is switched from a PV-driving mode. Firstly, the motor speed is controlled at a given speed in mode 3. At that point, J2 is turned on and J1 is off to switch to mode 1. By controlling the turn-off point, the maximum power of PV panel can be tracked. There are three steady working states for the double source (mode 1), as appeared in Figure 9. In Figure 9(a), S0 and S1 conduct, the PV panel charges the SRM winding to drive the motor; In Figure 9(b), S0 and S1 turn off; and the battery is charged with freewheeling current of the phase winding. Figure 9(c) appears a freewheeling state.

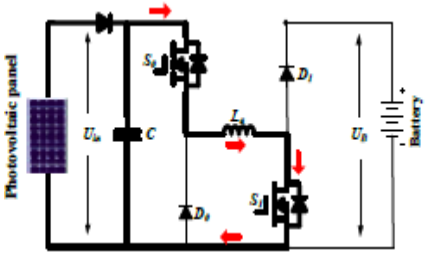

(a) Winding exciting state

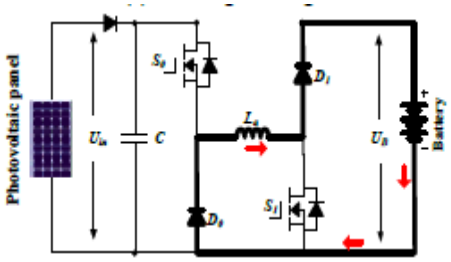

(b) Battery charging state

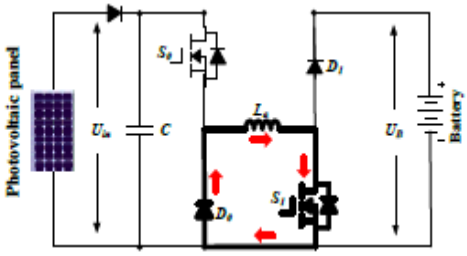

(c).Freewheeling state

Figure 9. Mode 1 working states.

Figure 10 is the control strategy under driving-charging mode. In Figure 10, θ_{on} is the turn on angle of SRM; θ_{off} is the turn-off angle of SRM. By changing turn-on angle, the speed of SRM can be controlled; the maximum power point tracking of PV panel can be achieved by adjusting turn-off angle, which can control the charging current to the battery.

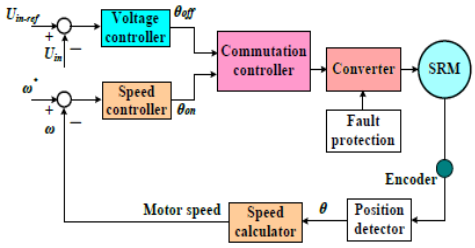

Figure 10. Control strategy under driving-charging mode (mode 1)

C. Grid-charging control system

The proposed topology also supports the single-phase grid charging. There are four fundamental charging states and S0 is dependably turned off. At the point when the grid instantaneous voltage is more than zero, the two working states are exhibited in Figure 11(a) and (b). In Figure 11(a), S1 and S2 conduct, the grid voltage charges the phase winding La2, the relating condition can be communicated as Eq.7; In Figure 11(b), S1 turns off and S2 conducts, the grid is associated in series with phase winding to charges the battery, the relating condition can be communicated as Eq. 8.

$$U_{grid} = L_{a2} \cdot \frac{di_{grid}}{dt} \quad (7)$$

$$U_B - U_{grid} = L_{a2} \cdot \frac{di_{grid}}{dt} \quad (8)$$

At the point when the grid instantaneous voltage is below zero, the two working states are introduced in Figure 11(c) and (d). In Figure 11(c), S1 and S2 conduct, the grid voltage charges the phase winding La1 and La2, the comparing condition can be communicated as Eq. (9); In Figure 11(d), S1 continues conducing and S2 turns off, the grid is associated in series with phase winding La1 and La2 to charges the battery, the relating condition can be communicated as Eq. 10.

$$U_{grid} = \frac{L_{a1} + L_{a2}}{L_{a1} \cdot L_{a2}} \cdot \frac{di_{grid}}{dt} \quad (9)$$

$$-U_B - U_{grid} = \frac{L_{a1} + L_{a2}}{L_{a1} \cdot L_{a2}} \cdot \frac{di_{grid}}{dt} \quad (10)$$

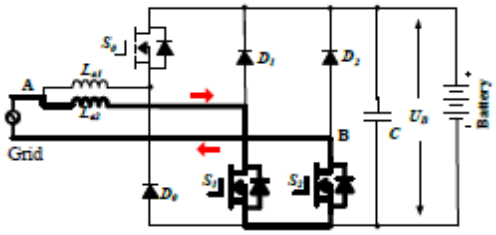

(a) Grid charging state 1 (*Ugrid*>0)

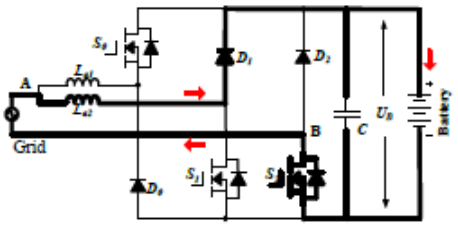

(b) Grid charging state 2 (*Ugrid*>0)

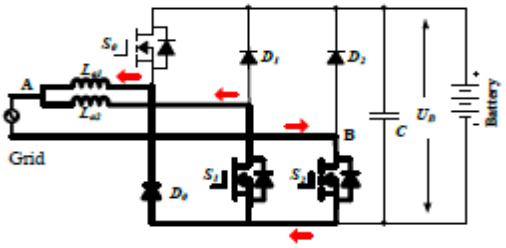

(c) Grid charging state 3 (*Ugrid*<0)

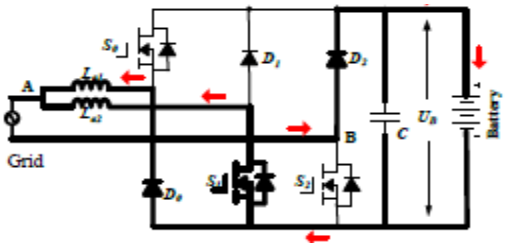

(e) Grid charging state 4 (*Ugrid*<0)

Figure 11. Mode 5 charging states .

In Figure 12, Ugrid is the grid voltage; by the phase lock loop (PLL), the phase data can be got; Iref_grid is the given amplitude of the grid current. Combining sinθ and Iref_grid, the instantaneous grid current reference iref_grid can be figured. In this mode, when Ugrid > 0, the inductance is La2; when Ugrid < 0, the inductance is paralleled La1 and La2; so in order to adopt the change in the inductance, hysteresis control is employed to acknowledge grid current regulation. Besides, hysteresis control has great loop performance, global stability and small phase lag that makes grid connected control stable

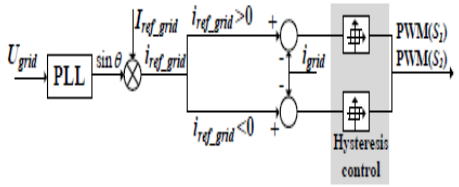

Figure 12. Grid-connected charging control (Mode 5).

D. PV-fed charging control system

In this mode, the PV panel charges the battery specifically by the driving topology. The phase windings are employed as inductor; what's more, the driving topology can be worked as interleaved Buck boost charging topology. For one phase, there are two states, as appeared in Figure 13(a) and (b). Whenever S0 and S1 turn on, the PV panel charges phase inductance; when S0 and S1 turns off, the phase inductance discharges energy to battery. According to the state-of-charging (SoC), there are three stages to make full utilize of solar energy and keep up battery healthy condition, as represented in Fig.13 (c). During stage 1, the relating battery SoC is in 0~SoC1, the battery is in greatly need energy condition, the MPPT control strategy is utilized to make full utilization of solar energy. During stage 2, the corresponding battery SoC is in SoC1~ SoC2, the constant voltage control is adapted to charging the battery. During stage 3, the corresponding battery SoC is in SoC2~1, the micro current charging is adapted. In order to simplify the control strategy, constant voltage is employed in PV panel MPPT control.

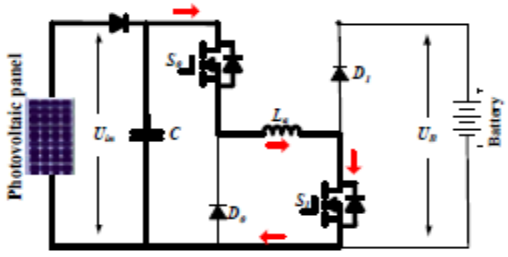

(a) Phase inductance charging

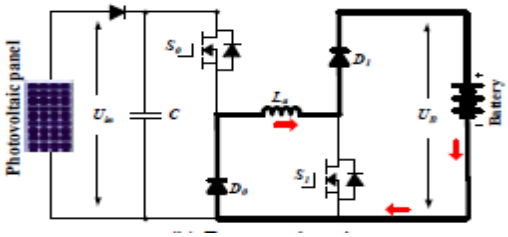

(b) Battery charging

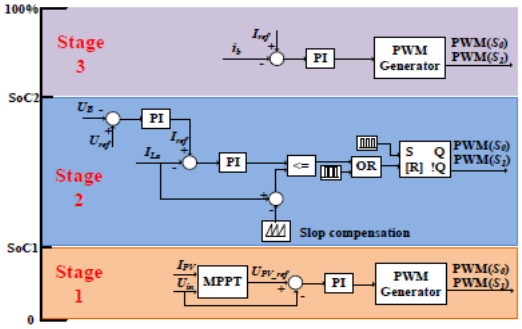

(c) Charging control strategy.

Figure 13. Mode 6 charging states and control strategy.

Extension:

Fuzzy Logic System:

Today control systems are usually described by mathematical models that follow the laws of physics, stochastic models or models which have emerged from mathematical logic. A general difficulty of such constructed model is how to move from a given problem to a proper mathematical model. Undoubtedly, today's advanced computer technology makes it possible; however managing such systems is still too complex.

These complex systems can be simplified by employing a tolerance margin for a reasonable amount of imprecision, vagueness and uncertainty during the modeling phase. As an outcome, not completely perfect system comes to existence; nevertheless in most of the cases it is capable of solving the problem in appropriate way. Even missing input information has already turned out to be satisfactory in knowledge-based systems.

Fuzzy logic allows to lower complexity by allowing the use of imperfect information in sensible way. It

can be implemented in hardware, software, or a combination of both. In other words, fuzzy logic approach to problems' control mimics how a person would make decisions, only much faster. Usually fuzzy logic control system is created from four major elements presented on Figure 1: fuzzification interface, fuzzy inference engine, fuzzy rule matrix and defuzzification interface. Each part along with basic fuzzy logic operations will be described in more detail below.

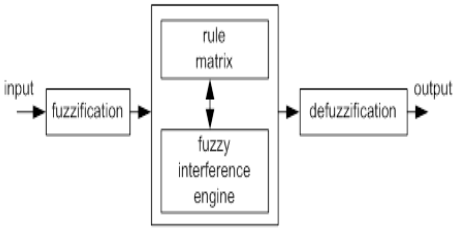

Figure 14. Fuzzy logic controller

IV. SIMULATION

A 12/8 SRM is initially modeled in Matlab/Simulink utilizing parameters in Table II. Figure 14(a) presents the simulation results at mode 1. The load torque is set as 35 Nm, the PV panel voltage is controlled at the MPP. The freewheeling current is used to charge the battery. Figure 14(b) demonstrates the simulation results of the single-source driving (modes 2-4).

Figure 15 demonstrates the simulation results of charging where Figure 15(a) is for grid-charging. The positive half current quality is superior to anything the negative half that is caused by the change in the grid-connected inductance. Fig.15(b) and (c) are for PV-charging. Figure 15(b) presents the step change from stage 1 to 2. In stage 1, the battery is low in SoC. In order to achieve MPPT of the PV, the constant voltage control is utilized and the PV output voltage is controlled at MPP (310 V), as appeared in Figure 15(b). In stage 2, a constant voltage is embraced; the reference voltage is set to 355 V. As appeared in Figure 15(b), the charging converter output voltage is controlled at reference voltage in the step change from stage 1 to stage 2. In stage 3, 1 A trickle charging is moreover accomplished, as appeared in Figure 15(c).

Mode 1

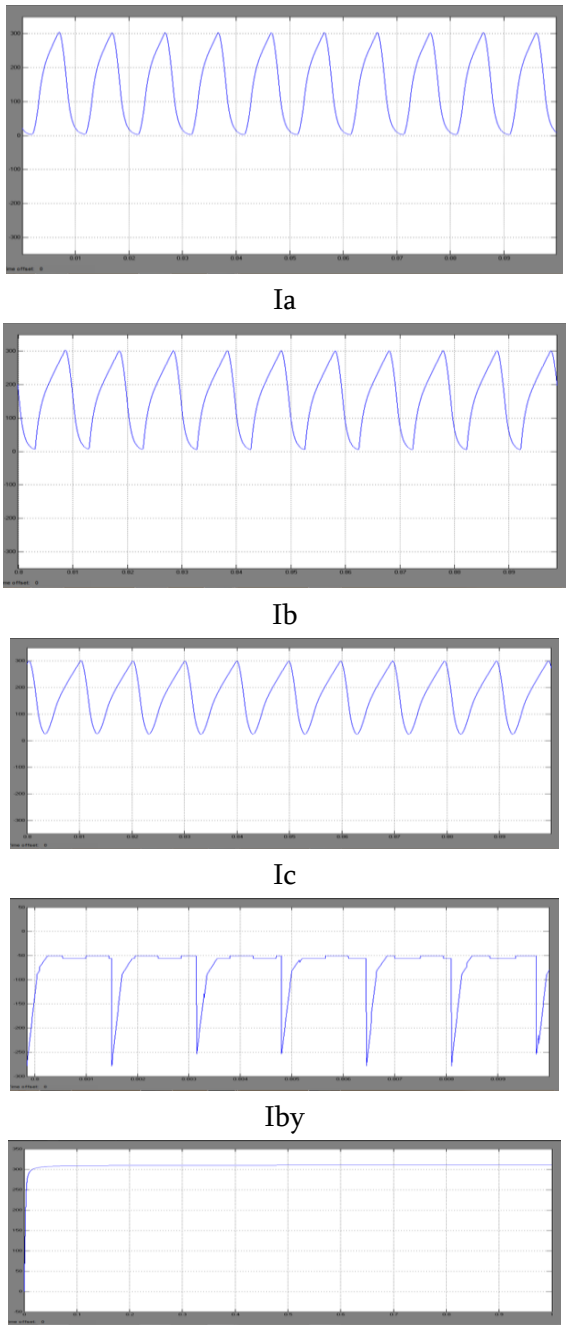

Ia

Ib

Ic

Iby

Uin

(a) Simulation results of driving-charging mode (mode 1)

Mode3

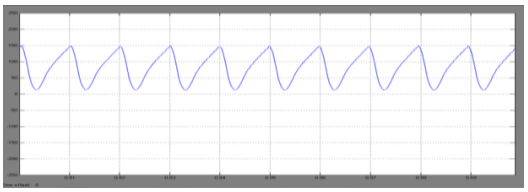

Ia

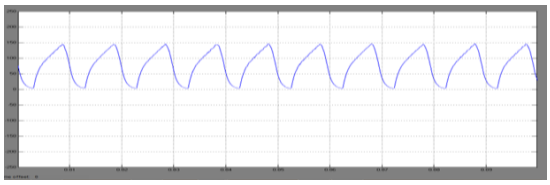

Ib

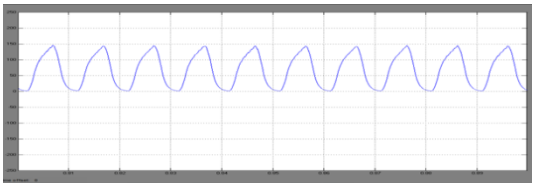

Ic

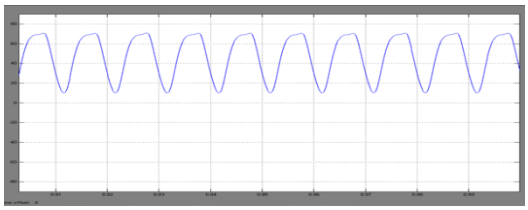

Torque

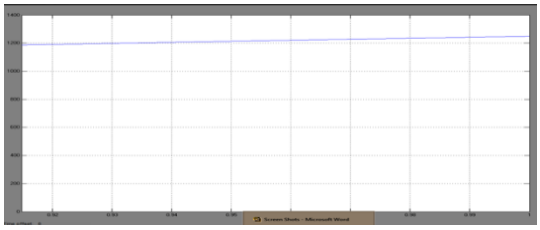

Speed

(b) Simulation results of single source driving mode (modes 3)

Figure 15 Simulation results for driving conditions at modes 1, 3 and 4.

Mode 5

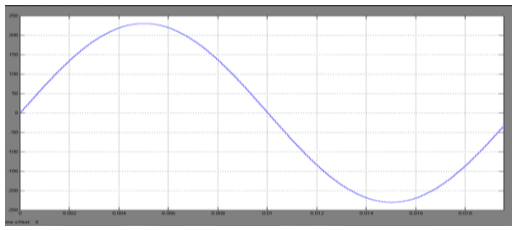

Ugrid

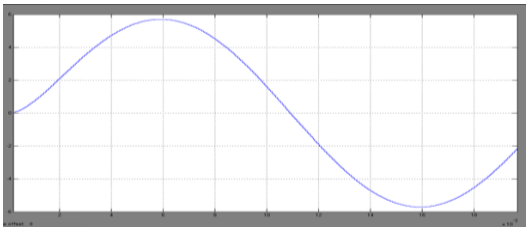

Igrid

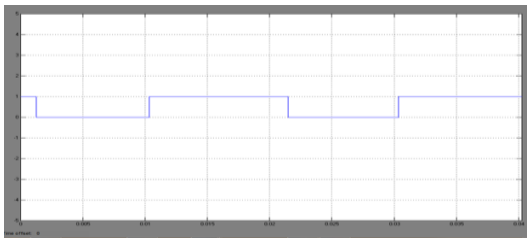

PWM1

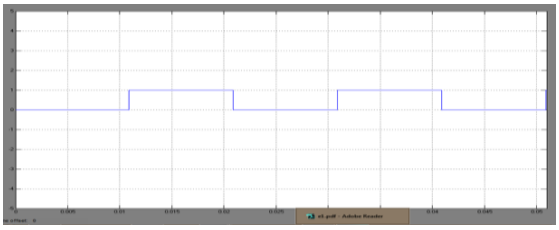

PWM2

(a) Grid charging (mode 5)

Mode6_Stage1

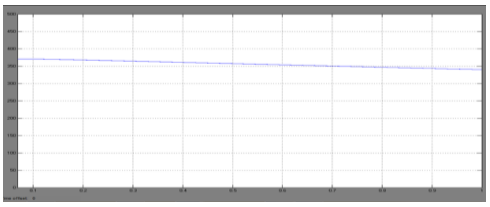

Ub

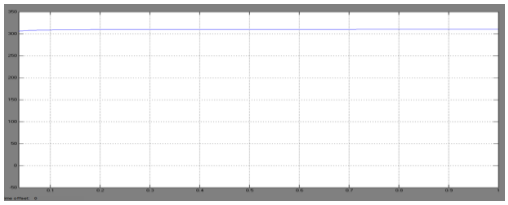

Uin

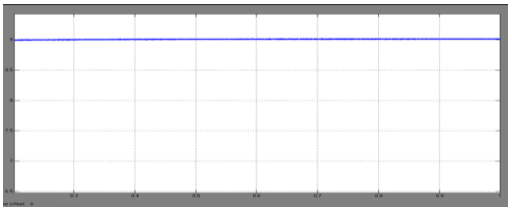

Ia

(b) PV charging mode 6 (stage 1)

Mode6_Stage2

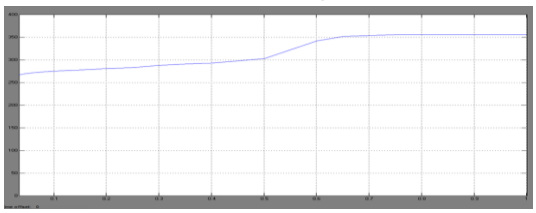

Ub

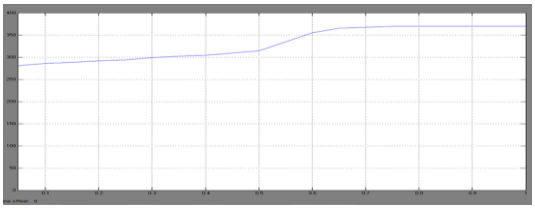

Uin

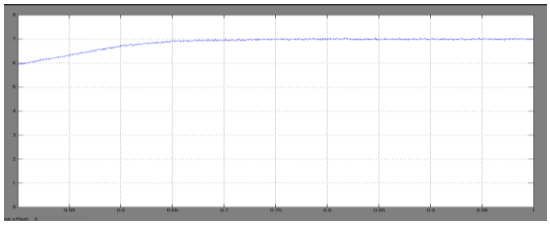

Ia

(c) PV charging mode 6 (stage 2)

Mode6_Stage3

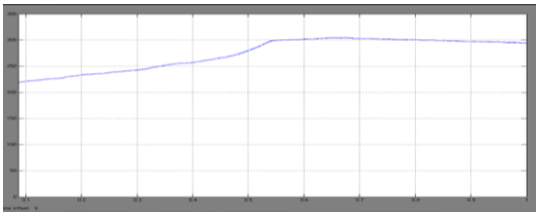

Ub

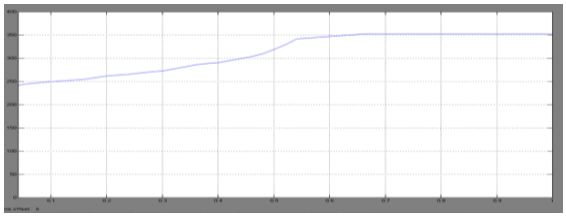

Uin

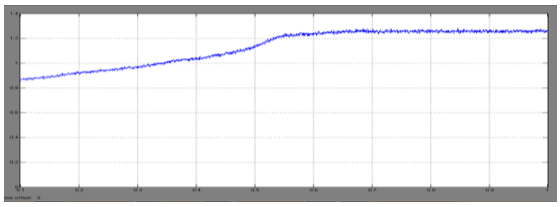

Iby

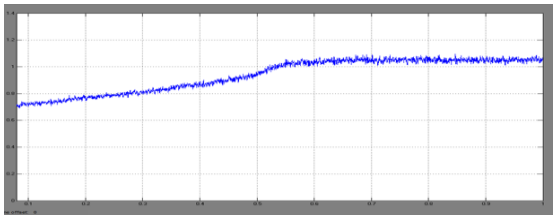

Ia

(d)PV charging mode 6 (stage 3)

Figure 16. simulation results for charging modes.

Table 1. THD values for Proposed and Extension methods.

THD in % proposed method	THD in % extension method
Mode 1: I_a = 41.43, I_b =38.12, I_c=64.58	Mode 1: I_a = 25.72, I_b =19.82, I_c=27.17
Mode 2: I_a = 43, I_b =31.01, I_c=71.52	Mode 2: I_a= 25.29 , I_b =14.46 , I_c=27.94
Mode 3: I_{La}= 82.66, I_{Lb} =33.68, I_{Lc}=43.47	Mode 3: I_{La}= 51.25, I_{Lb} =17.51, I_{Lc}=18.26
Mode 4: I_{La}= 64.68, I_{Lb} =34.25, I_{Lc}=41.87	Mode 4: I_{La}= 40.1, I_{Lb} =17.51, I_{Lc}=17.56
Mode 5: U_{grid} = 0.004535, I_{grid} =0.004864	Mode 5: U_{grid} = 0.004535, I_{grid}=0.004864
Mode 6:stage 1 I_a= 11.5	Mode 6:stage 1 I_a= 5.982
Mode 6:stage 2 I_{La}= 2.377	Mode 6:stage 2 I_{La}= 0.9965
Mode 6:stage 3 I_a= 2.429, I_b=2.632	Mode 6:stage 3 I_a= 1.815, I_b=1.969

V. CONCLUSION

In order to handle the range anxiety of utilizing EVs and decrease the system cost, a mix of the PV panel and SRM is proposed as the EV driving system.
The main contributions of this paper are:

(i) A tri-port converter is utilized to coordinate the PV panel, battery and SRM.

(ii) Six working modes are developed to achieve flexible energy flow for driving control, driving/charging hybrid control and charging control.
(iii) A novel grid-charging topology is formed without a need for external power electronics devices.
(iv) A PV-fed battery charging control scheme is developed to enhance the solar energy utilization.

Since PV-fed EVs are a greener and more economical innovation than conventional ICE vehicles, this work will give feasible solution to reducing the total costs and CO2 emissions of electrified vehicles. Moreover, the proposed innovation may likewise be connected to comparable applications, such as fuel cell powered EVs. Fuel cells have a considerably higher power density and are hence more qualified for EV applications.

VI. REFERENCES

1. A. Emadi, L. Young-Joo, K. Rajashekara, "Power electronics and motor drives in electric, hybrid electric, and plug-in hybrid electric vehicles," IEEE Trans. Ind. Electron., vol. 55, no. 6, pp. 2237-2245, Jun. 2008.
2. B. l. K. Bose, "Global energy scenario and impact of power electronics in 21st century," IEEE Trans. Ind. Electron., vol. 60, no. 7, pp. 2638-2651, Jul. 2013.
3. J. de Santiago, H. Bernhoff, B. Ekergård, S. Eriksson, S. Ferhatovic, R. Waters, and M. Leijon,"Electrical motor drivelines in commercial all-electric vehicles: a review," IEEE Trans. Veh. Technol., vol. 61, no. 2, pp. 475-484, Feb. 2012.
4. Z. Amjadi, S. S. Williamson, "Power-electronics-based solutions for plug-in hybrid electric vehicle energy storage and management systems," IEEE Trans. Ind. Electron., vol. 57, no. 2, pp. 608-616, Feb. 2010.
5. A. Kuperman, U. Levy, J. Goren, A. Zafransky, and A. Savernin, "Battery charger for electric vehicle traction battery switch station," IEEE Trans. Ind. Electron., vol. 60, no. 12, pp. 5391-5399, Dec. 2013.